Electronic Supplementary Material (ESI) for Chemical Communications.

Chromenopyrazole-Based Bipolar Host Materials for Solution-Processable Thermally Activated Delayed Fluorescence OLEDs Exhibiting High Efficiency and Low Roll-off

Mallesham Godumala, Jiwon Yoon, Chiho Lee, Ji-Eun Jeong, Sungnam Park, Han Young Woo, Min Ju Cho and Dong Hoon Choi*

Department of Chemistry, Research Institute for Natural Sciences, Korea University, 145 Anam-ro, Sungbuk-gu, Seoul 02841, Korea

*Corresponding author: dhchoi8803@korea.ac.kr

Table of Contents

1. Instrumentation, Materials, and Synthesis

1-1. Instrumentation

^{1}H and ^{13}C nuclear magnetic resonance (NMR) spectra were recorded on Varian Mercury 500 MHz spectrometers in $CDCl_3$ solvent (Cambridge Isotope Laboratories, Inc.) using tetramethylsilane (TMS) as the internal standard. An EA1112 elemental analyzer (Thermo Electron Corporation) was used to carry out elemental analyses. A Bruker Daltonics LRF-20 MALDI-TOF mass spectrometer was used to obtain the molecular weight information of the compounds. The glass transition temperatures (T_g) of the hosts were examined using a Mettler 821 differential scanning calorimetry (DSC) instrument under a nitrogen atmosphere at a heating rate of 10 °C min^{-1}. Thermogravimetric analysis using TGA, Mettler STAR^e was performed at a heating rate of 10 ^{o}C min^{-1} under nitrogen atmosphere. Atomic force microscopy (AFM; Advanced Scanning Probe Microscope, XE-100, PSIA), operating in the tapping mode with a silicon cantilever, was used to examine the surface morphologies of the emissive layers. For this purpose, film samples were prepared by a solution process with 5 wt% dopant concentration, similar to the optimized conditions of the OLEDs. The absorption spectra were recorded on a UV-Vis spectrophotometer (Agilent 8453, λ = 190–1100 nm). The fluorescence and low-temperature PL spectra were measured using Hitachi F-7000 fluorescence spectrophotometer. The PL quantum yield (PLQY) was obtained using the JASCO FP-8500 fluorescence spectrometer equipped with an integrated sphere. The transient PL measurements at room temperature (RT) were evaluated for doped films (5 wt% dopant concentration) of **DCzCP**:t4CzIPN, **TCzCP**:t4CzIPN, and mCP:t4CzIPN under nitrogen atmosphere. For this purpose, blend films (dopant concentration of 5.0 wt% with the film thickness of 20 nm) were prepared on a quartz plate using toluene. The PL decays were measured between 0 and 50 μs. The exciton lifetimes and transient PL were measured with a train of 1064-nm pulses of 5 ns duration, produced at 10 Hz from a Nd:YAG laser (Powerlite Precision II 8000, Continuum). A 355-nm pulse was obtained by the generation of the third harmonic and used to directly excite the film sample cast on quartz. The emission from the film sample was collected using a lens (focal length: 10 cm), passed through a monochromator, and detected using a photomultiplier tube (PMT) connected to a 100 MHz digital oscilloscope (DSO-X 3014A, Keysight). The prompt and delayed components were identified using single- and triple-exponential decaying functions. Cyclic voltammetry was utilized to measure the oxidation potentials of the hosts in their film state using a potentiostat (EA161, eDAQ) at a scan rate of 50 mV s^{-1}. For this purpose, freshly prepared 0.1 M tetrabutylammonium hexafluorophosphate (NBu_4PF_6) in dry acetonitrile was used as the electrolytic solution. Pt wire (diameter:

0.5 mm) and Ag/AgCl electrodes were used as counter and reference electrodes, respectively, and the film was prepared by drop-casting form methylene chloride solution on Pt electrode.

1-2. Materials

All reagents and solvents were purchased from Alfa Aesar, TCI, and Aldrich and used without further purification unless otherwise stated. 8-Bromo-3-methyl-1-phenylchromeno[4,3-c]pyrazol-4(1H)-one (Br-CP)[1] and 9,9'-(5-bromo-1,3-phenylene)bis(9H-carbazole)[2] were synthesized using methods previously reported in the literature. The other key intermediates such as TCzBr and BA-CP were synthesized, and the conditions required for the Suzuki reaction between bromo-derivatives and BA-CP were probed to yield the target molecules as described below (Schemes 1 and S1).

1-3. Synthesis

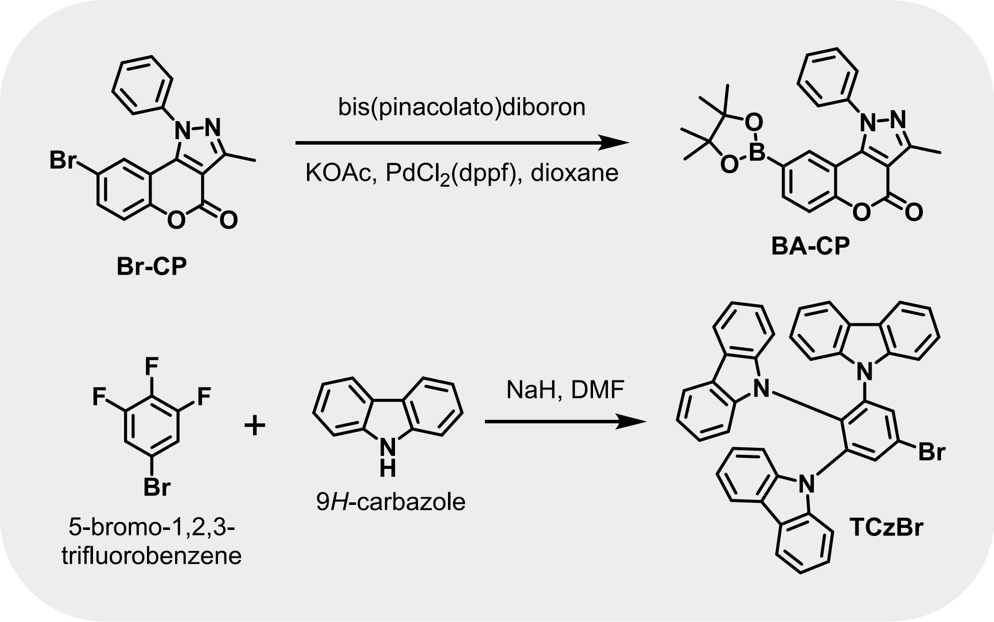

Scheme S1 Synthetic route of key intermediates.

Synthesis of 3-methyl-1-phenyl-8-(4,4,5,5-tetramethyl-1,3,2-dioxaborolan-2-yl)chromeno [4,3-c]pyrazol-4(1H)-one (BA-CP)

Br-CP (3.0 g, 8.5 mmol), 4,4,4',4',5,5,5',5'-octamethyl-2,2'-bi(1,3,2-dioxaborolane) (4.3 g, 17.0 mmol), [l,l'-bis(diphenylphosphino)ferrocene]dichloropalladium (PdCl$_2$(dppf)) (0.2 g, 0.25 mmol), and anhydrous potassium acetate (KOAc) (2.4 g, 25.4 mmol) were mixed in 1,4-dioxane (60 mL) before purging with nitrogen gas for 20 min. The reaction mixture was stirred at 100 °C for 8 h, and the reaction progress was monitored by thin layer chromatography (TLC). After complete conversion, it was cooled to RT, filtered through Celite, and concentrated under reduced pressure. The residue obtained was subjected to silica-gel column chromatography using ethyl acetate (EA):hexane (20:80) as the eluent to obtain BA-CP as a white solid (3.0 g, 88% yield). ^{1}H NMR (500 MHz, $CDCl_3$): δ (ppm) 7.84-7.80 (dd, *J* = 8.4, 1.4 Hz, 1H), 7.63-7.55 (m, 6H), 7.38 (d, *J* = 8.2 Hz, 1H), 2.69 (s, 3H), 1.25 (s, 12H). ^{13}C NMR (125 MHz, $CDCl_3$): δ (ppm) 157.86, 155.22, 150.77, 141.68, 139.29, 136.92, 129.85, 129.70, 129.68, 126.84, 117.22, 111.27, 106.25, 83.98, 24.78, 12.89.

Synthesis of 9,9',9''-(5-bromobenzene-1,2,3-triyl)tris(9H-carbazole) (TCzBr)

Sodium hydride (0.69 g, 18.0 mmol) was added to 9H-carbazole (2.5 g, 15.0 mmol) in DMF (20 mL) at RT. After 30 min, 1-bromo-3,4,5-trifluorobenzene (0.54 mL, 4.5 mmol) dissolved in DMF (5 mL) was added dropwise at RT, and the mixture was heated to 70 °C for 6 h. After cooling to RT, water was added, and the organic compound was extracted in EA. The combined organic extracts were dried, concentrated, and precipitated in methanol to ascertain TCzBr as a white solid (1.5 g, 51.3% yield). ^{1}H NMR (500 MHz, $CDCl_3$): δ (ppm) 8.08 (s, 2H), 7.77-7.73 (m, 4H), 7.37-7.33 (m, 2H), 7.22-7.18 (m, 4H), 7.07-7.00 (m, 8H), 6.92-6.88 (m, 2H), 6.78-6.72 (td, *J* = 7.5, 0.9 Hz, 2H), 6.66-6.61 (ddd, *J* = 8.3, 7.2, 1.2 Hz, 2H). ^{13}C NMR (125 MHz, $CDCl_3$): δ (ppm) 139.53, 138.39, 138.10, 132.59, 125.47, 124.60, 123.63, 123.47, 121.86, 120.40, 119.96, 119.88, 119.36, 109.79, 109.69.

Synthesis of 8-(3,5-di(9H-carbazol-9-yl)phenyl)-3-methyl-1-phenylchromeno[4,3-c]pyrazol-4(1H)-one (DCzCP)

A mixture of BA-CP (0.5 g, 1.24 mmol), 9,9'-(5-bromo-1,3-phenylene)bis(9H-carbazole) (0.6 g, 1.24 mmol), and K_2CO_3 (0.5 g, 3.73 mmol) dissolved in THF:H_2O solvent mixture (3:1, 16 mL) was purged with nitrogen for 15 min. Subsequently, $Pd(PPh_3)_4$ (43 mg, 0.037 mmol) was added as the a catalyst, and the mixture was purged again with nitrogen for 10 min. The temperature of the reaction mixture was raised to 65 °C, and stirred for 3 h. After cooling to room temperature, the organic layer was extracted in methylene chloride (MC), dried, filtered, and subjected to silica-gel column chromatography using hexane:MC (1:1, *v/v*) to MC only as the eluent. The obtained compound was further purified by precipitating in hot toluene to yield **DCzCP** as a white solid (0.74 g, 87% yield). ^{1}H NMR (500 MHz, $CDCl_3$): δ (ppm) 8.21-8.17 (m, 4H), 7.83-7.80 (dd, *J* = 8.7, 2.3 Hz, 1H), 7.75 (t, *J* = 1.8 Hz, 1H), 7.57 (d, *J* = 1.8 Hz, 2H), 7.52 (d, *J* = 8.9 Hz, 1H), 7.49-7.44 (m, 10H), 7.38-7.33 (m, 5H), 7.17-7.12 (m, 2H), 6.77-6.72 (tt, *J* = 7.6, 1.1 Hz, 1H), 2.69 (s, 3H). ^{13}C NMR (125 MHz, $CDCl_3$): δ (ppm) 157.62, 153.30, 150.98, 142.19, 141.42, 140.68, 140.15, 138.99, 134.12, 130.40, 129.80, 129.16, 126.72, 126.29, 124.80, 123.86, 123.67, 120.69, 120.57, 120.54, 118.82, 112.37, 109.64, 106.50, 12.90. MS (MALDI-TOF) [m/z]: Calcd for $C_{47}H_{30}N_4O_2$, 682.237; Found, 682.263 [M^+]. Elemental analysis (%) calcd for $C_{47}H_{30}N_4O_2$: C 82.68, H 4.43, N 8.21. Found: C 82.77, H 4.49, N 8.16.

Synthesis of 3-methyl-1-phenyl-8-(3,4,5-tri(9H-carbazol-9-yl)phenyl)chromeno[4,3-c] pyrazol-4(1H)-one (TCzCP).

TCzCP was obtained as a white solid (0.91 g, 86% yield) from BA-CP (0.5 g, 1.24 mmol), TCzBr (0.8 g, 1.24 mmol), and K_2CO_3 (0.5 g, 3.73 mmol) under reaction conditions similar to those required for the synthesis of **DCzCP**. ^1H NMR (500 MHz, $CDCl_3$): δ (ppm) 7.90-7.86 (m, 1H), 7.87-7.83 (m, 4H), 7.79 (s, 2H), 7.56 (d, *J* = 8.9 Hz, 1H), 7.45-7.43 (m, 2H), 7.41-7.37 (m, 2H), 7.37 (d, *J* = 2.1 Hz, 1H), 7.20-7.16 (m, 4H), 7.12-7.04 (m, 8H), 7.00 (d, *J* = 8.2 Hz, 2H), 6.99-6.95 (m, 2H), 6.81-6.76 (td, *J* = 7.5, 0.9 Hz, 2H), 6.71-6.67 (td, *J* = 8.2, 1.4 Hz, 2H), 6.54-6.48 (tt, *J* = 7.6, 1.2 Hz, 1H), 2.71 (s, 3H). ^{13}C NMR (125 MHz, $CDCl_3$): δ (ppm) 157.56, 153.39, 150.96, 141.37, 139.87, 139.79, 138.87, 138.41, 138.03, 133.04, 131.37, 130.40, 129.71, 128.83, 127.10, 126.67, 125.49, 124.56, 123.60, 123.47, 120.59, 120.26, 120.00, 119.84, 119.40, 118.94, 112.47, 109.95, 109.79, 106.45, 12.91. MS (MALDI-TOF) [m/z]: Calcd for $C_{59}H_{37}N_5O_2$, 847.295; Found, 847.260 [M^+]. Elemental analysis (%) calcd for $C_{59}H_{37}N_5O_2$: C 83.57, H 4.40, N 8.26. Found: C 83.68, H 4.51, N 8.19.

2.0 Theoretical calculations

Time-dependent density functional theory (TD-DFT) calculations using Gaussian 09 program at B3LYP/6-31G* basis level were performed to obtain their optimized geometries and HOMO and LUMO distributions (Fig. S1). The HOMO and LUMO values were determined to be −5.55 and −1.66 eV for **DCzCP** and −5.47 and −1.73 eV for **TCzCP**, respectively. The realistic shallower HOMO and deeper LUMO levels for **TCzCP** are attributed to the increased number of electron-donating carbazole units.

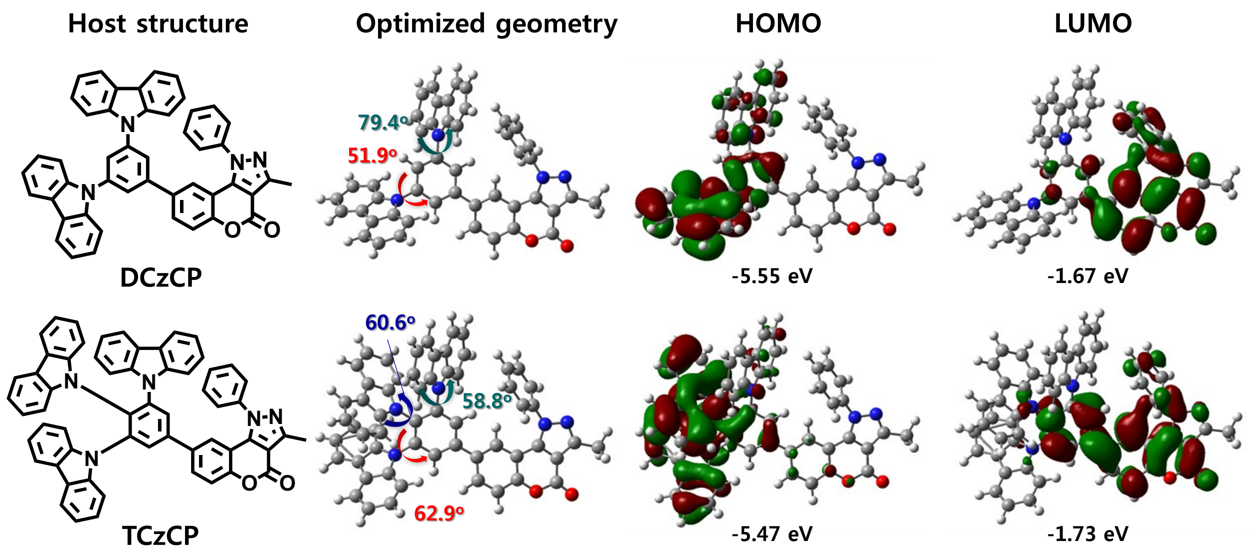

Fig. S1 Chemical structure, optimized geometry, and HOMO and LUMO spatial distributions of **DCzCP** and **TCzCP** calculated at the B3LYP/6-31G (DFT) level of theory with Gaussian 09W.

3.0 Thermal and morphological properties

A high glass transition temperature (T_g) is essential for application in OLEDs as this ensures the formation of smooth amorphous films during device fabrication and thus improves the device performance and its lifetime.

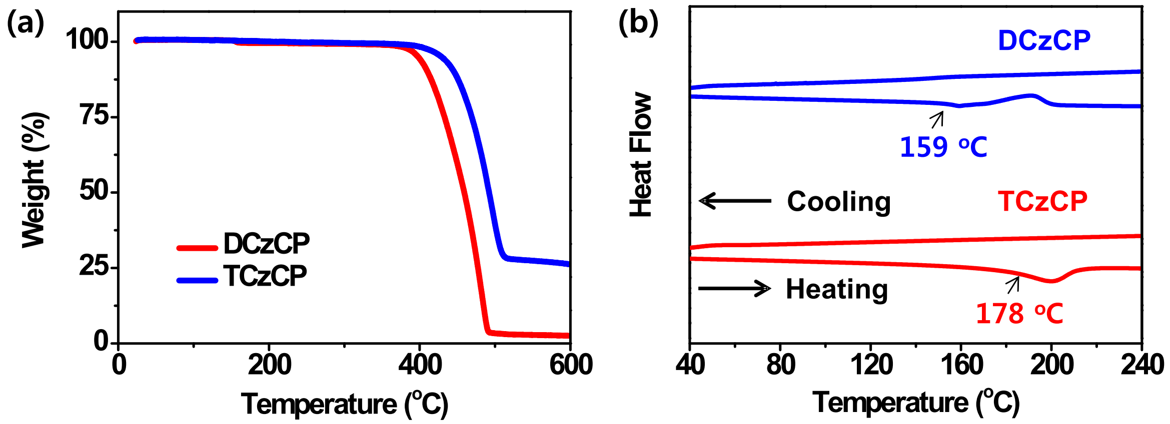

Fig. S2 (a) TGA and (b) DSC thermograms of **DCzCP** and **TCzCP.**

The thin films for AFM measurements were prepared by spin-coating the blend solution of **DCzCP**:t4CzIPN, **TCzCP**:t4CzIPN, and mCP:t4CzIPN on glass/PEDOT:PSS. The dopant concentration was 5 wt% and the film thickness was 50 nm. Notably, the smallest RMS value was observed for **DCzCP**, signifying that it can produce homogeneous films during device fabrication, which is one of the predominant factors to realize high device performances.

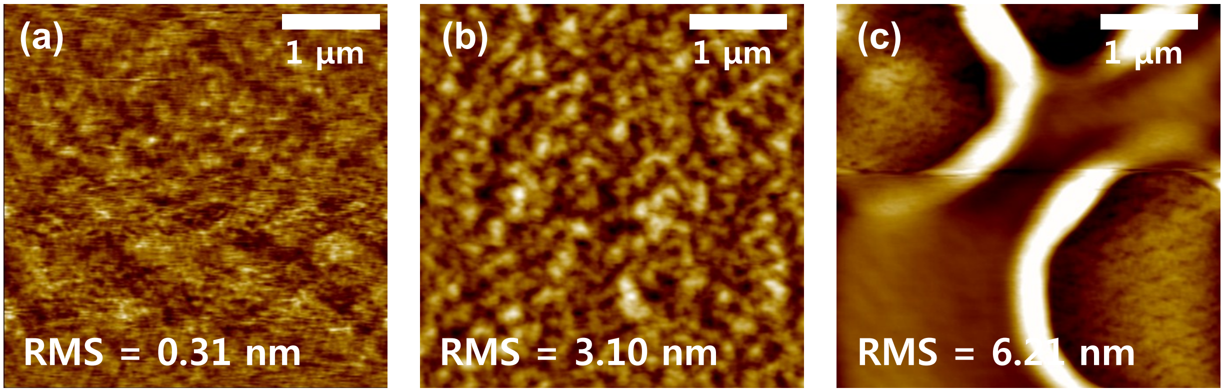

Fig. S3 AFM topographic images (5 x 5µm) of blend films of (a) **DCzCP:t4CzIPN,** (b) **TCzCP:t4CzIPN** and (c) **mCP:t4CzIPN.**

4.0 Photophysical properties

The two compounds have similar absorption profiles in dilute solution and film states indicating the absence of considerable intermolecular interactions in the ground state. Both compounds do not exhibit any solvatochromic effects during UV-Vis absorption measurements in different polar environments designating negligible dipole moment change in the ground state (Fig. S4).

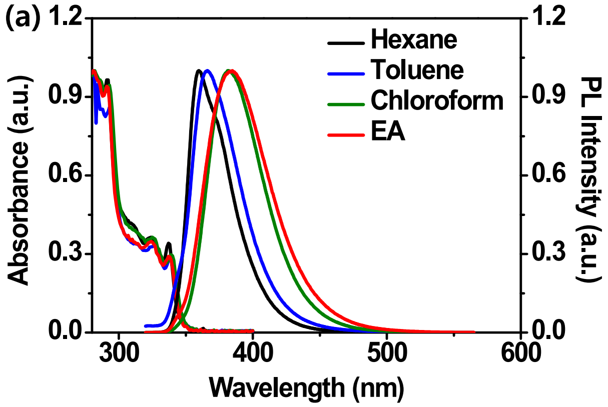

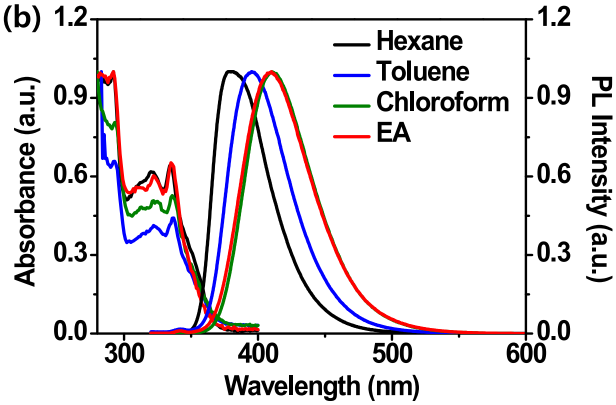

Fig. S4 UV-Vis absorption and photoluminescence spectra of (a) **DCzCP**, and **(b) TCzCP** in different polar solvents.

Table S1 UV-Vis absorption and PL data in different polar solvents

compound	Hexane (nm) [a/b]	Toluene (nm) [a/b]	$CHCl_3$ (nm) [a/b]	EA (nm) [a/b]
DCzCP	291, 324, 337/360	293, 326, 339/366	293, 322, 339/382	291, 324, 337/385
TCzCP	292, 320, 335/380	293, 322, 337/395	294, 322, 336/410	294, 322, 335/410

[a] Absorbance. [b] PL value.

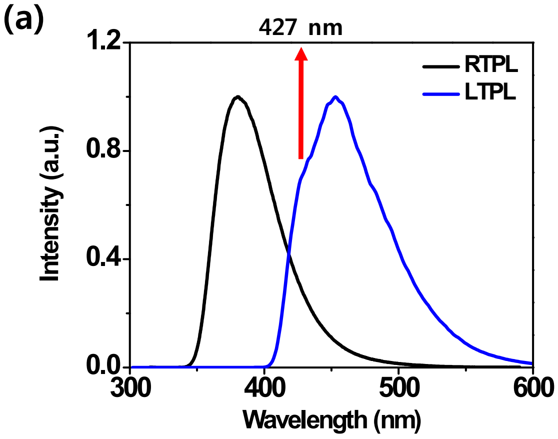

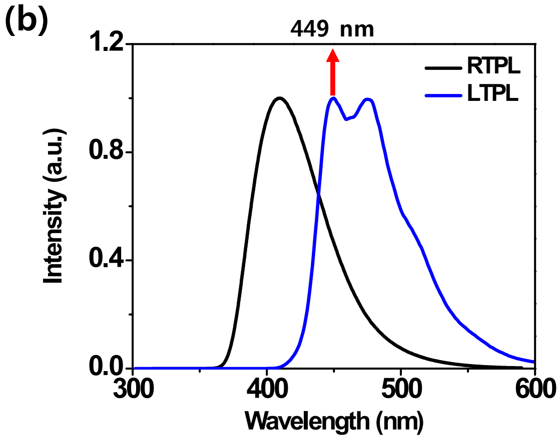

Fig. S5 Room-temperature and low-temperature PL spectra of (a) **DCzCP**, and (b) **TCzCP** in 2-methyltetrahydrofuran solution.

Absorption spectra of **t4CzIPN** and PL spectra of **DCzCP** and **TCzCP** are shown in Fig. S6a. Fig. S6b shows the PL spectrum of **t4CzIPN**. To verify energy transfer efficiency from host to dopant, PL spectra were measured for mixed films of **DCzCP**: **t4CzIPN** and **TCzCP**: **t4CzIPN** at 5.0 wt% dopant concentration. As shown in Fig. S6c and S6d, efficient energy transfer from the Cz-based host to **t4CzIPN** can be observed. In particular, the energy transfer efficiency from **DCzCP** to dopant was observed to be higher than in **TCzCP**. These results can be evidence that **DCzCP**-based devices can expect higher efficiency than **TCzCP**-based devices. As a result, the high energy transfer efficiency of **DCzCP**: **t4CzIPN** contributed to improving the EQE of TADF-OLED compared to **TCzCP**: **t4CzIPN**.

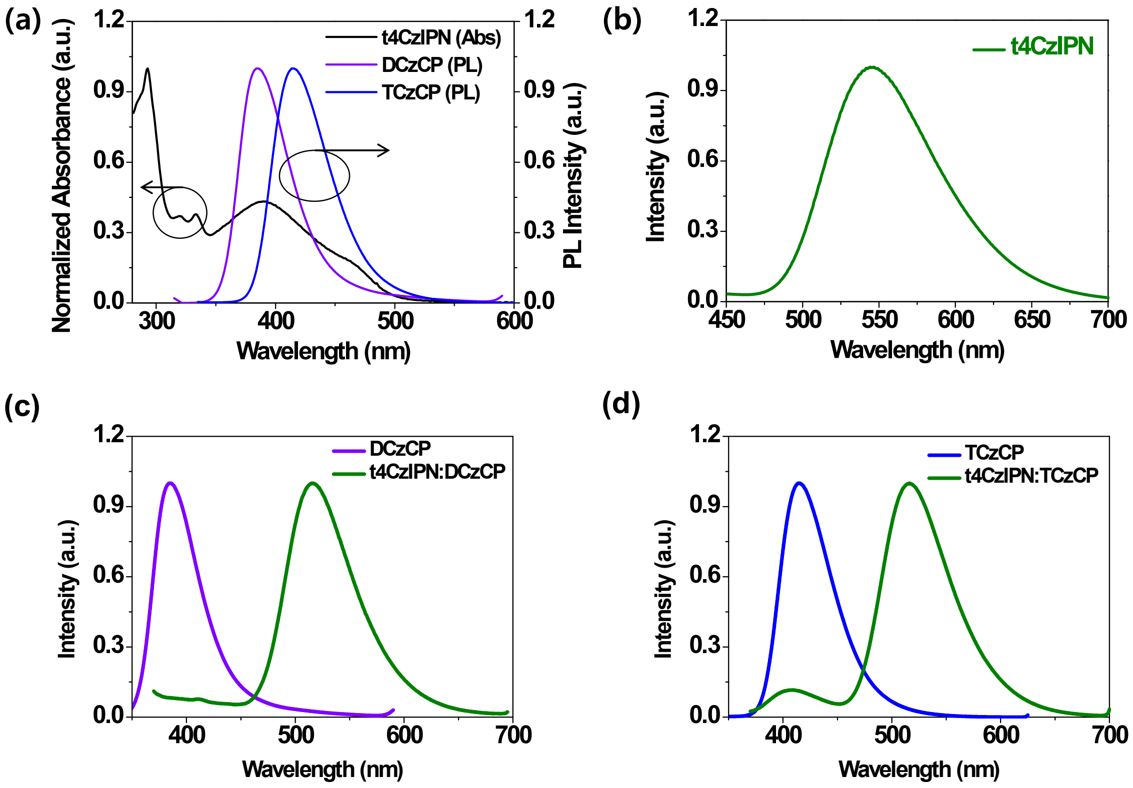

Fig. S6 UV–Vis absorption spectra of t4CzIPN emitter and PL spectra of DCzCP and TCzCP hosts in the film state (a), and PL spectrum of t4CzIPN in the film state (b). PL spectra of the DCzCP:t4CzIPN (c) and TCzCP:t4CzIPN (d) films on quartz and excitation wavelength of 355 nm.

5.0 Transient PL and kinetic parameters

Transient PL (TRPL) decay studies were probed to investigate the TADF characteristics of t4CzIPN doped into **DCzCP**, **TCzCP**, and **mCP** thin films under nitrogen atmosphere. Kinetic parameters including the radiative decay rate constant of the singlet excited state (k_r^S), rate constant for intersystem crossing (ISC) from the singlet excited to the triplet excited state (k_{ISC}), rate constant for RISC from the triplet excited state to the singlet excited state (k_{RISC}), and non-radiative (nr) decay rate constant for the triplet excited state (k_{nr}^T) were calculated (Table S2),. The k_p and k_d are the prompt and delayed fluorescence decay rate constants calculated from the corresponding prompt and delayed lifetimes ($k_p = 1/\tau_p$ and $k_d = 1/\tau_d$). The τ_p and τ_d values were evaluated by fitting a double-exponential decay mode $I(t) = A_1 \exp(-t/\tau_p) + A_2 \exp(-t/\tau_d)$, where A_1 and A_2 are fitting parameters.[3] The rate constants were calculated using the following equations:

$$k_r^S = k_p \cdot \Phi_p \qquad (1)$$

$$k_{ISC} = k_p \cdot (1 - \Phi_p) \qquad (2)$$

$$k_{RISC} = (k_p \cdot k_d / k_{ISC}) \cdot (\Phi_d / \Phi_p) \qquad (3)$$

$$k_{nr}^T = k_d - k_{RISC} \cdot \Phi_p \qquad (4)$$

The non-radiative decay rate constant of the singlet excited state (k_{nr}^S) is zero at 300 K.[4–5]

Table S2 Photophysical properties and kinetic parameters of t4CzIPN-doped (5.0 wt%) DCzCP, TCzCP, and mCP films

Comp	τ_p (ns)[a]	τ_d (μs)[b]	Φ_{PL} (%)[c]	Φ_p (%)[d]	Φ_d (%)[e]	k_p ($\times 10^7$ s^{-1})[f]	k_d ($\times 10^5$ s^{-1})[g]	k_r^S ($\times 10^7$ s^{-1})[h]	k_{ISC} ($\times 10^7$ s^{-1})[i]	k_{RISC} ($\times 10^5$ s^{-1})[j]	k_{nr}^T ($\times 10^5$ s^{-1})[k]
DCzCP	15.19	3.10	65.48	15.78	49.70	6.58	3.22	1.04	5.54	12.0	1.32
TCzCP	13.04	2.92	66.68	19.40	47.28	7.67	3.42	1.49	6.18	10.3	1.41
mCP	17.45	2.63	57.90	15.83	42.07	5.73	3.80	0.91	4.82	12.0	1.90

[a] Prompt emission lifetime. [b] Delayed emission lifetime. [c] Absolute PLQY measured with an integrating sphere. [d] PLQY of the prompt emission estimated according to the corresponding proportions in the transient decay curve. [e] PLQY of the delayed emission estimated according to the corresponding proportions in the transient decay curve. [f] Prompt emission rate constant. [g] Delayed emission rate constant. [h] Radiative decay rate constant of the singlet excited state. [I] Intersystem crossing rate constant. [j] Reverse intersystem crossing rate constant. [k] Non-radiative decay rate constant

for triplet excited state.

The ISC rate constant (k_{ISC}) of **DCzCP**: t4CzIPN film was calculated to be 5.54 × 10^7 s^{-1}, which is lower than TCzCP: t4CzIPN film (6.18 × 10^7 s^{-1}). RISC rate constants (k_{RISC}) of **DCzCP**: t4CzIPN and **TCzCP**: t4CzIPN films were determined to be 12.0 × 10^5 s^{-1} and 10.3 x 10^5 s^{-1}. Based on these results, we expected **DCzCP**-based OLEDs to be more efficient than **TCzCP**-based OLEDs.

6.0 Electrochemical properties

The HOMO energy was calculated from the E_{ox}^{onset} values and referenced to ferrocene using the equation: HOMO (eV) = $-e$ (4.8 + E_{ox}^{onset} − $E_{Fc/Fc+}$),[6] where the Fc/Fc⁺ potential is +0.36 V.

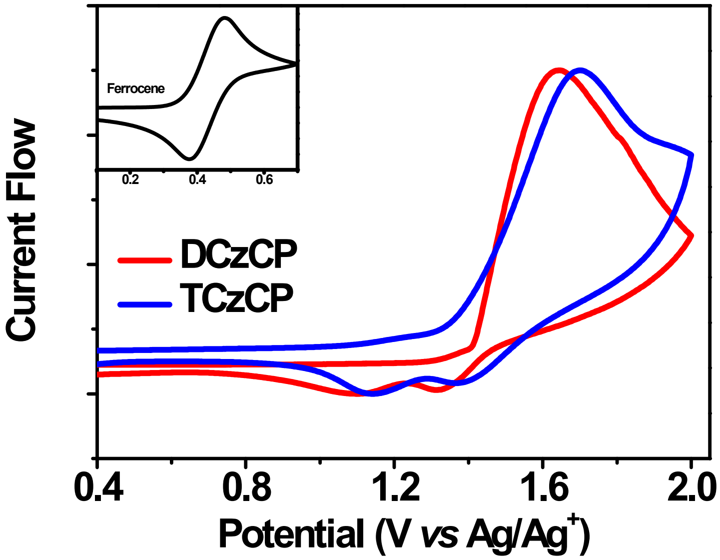

Fig. S7 cyclic voltammograms of the two hosts in film state (inset shows the cyclic voltammogram of ferrocene).

7.0 Single carrier devices

Single-carrier devices like hole-only devices (HODs) and electron-only devices (EODs) were prepared using a clean glass substrate coated with indium tin oxide (ITO, 150 nm) layer as the anode, with a sheet resistance of 10 Ω cm^{-2}. The active pattern size was 2 × 2 mm^2. HODs with the configuration of ITO (150 nm)/poly(3,4-ethylenedioxy thiophene) polystyrene sulfonate (PEDOT:PSS) (40 nm)/poly(9-vinyl carbazole) (PVK) (10 nm)/**Host** (20 nm)/Aluminum (Al) (100 nm), and EODs with the configuration of ITO (150 nm)/**Host** (20 nm)/2,2′,2"-(1,3,5-benzinetriyl)-tris(1-phenyl-1-H-benzimidazole (TPBi) (40 nm)/ lithium fluoride (LiF) (0.8 nm)/ Al (100 nm) were fabricated for **DCzCP** and **TCzCP** hosts and compared with mCP. PEDOT:PSS, PVK, and host materials were deposited by spin coating, whereas TPBi, LiF, and Al were deposited using a vacuum thermal evaporator. PEDOT:PSS and PVK function as the hole injection and transport layers, respectively, in the HODs, while TPBi and LiF act as electron injection and transport layers, respectively, in the EODs. ITO and Al are the anode and cathode, respectively. The current density-voltage (*J*-*V*) data were measured using a Keithley SMU 236 system.

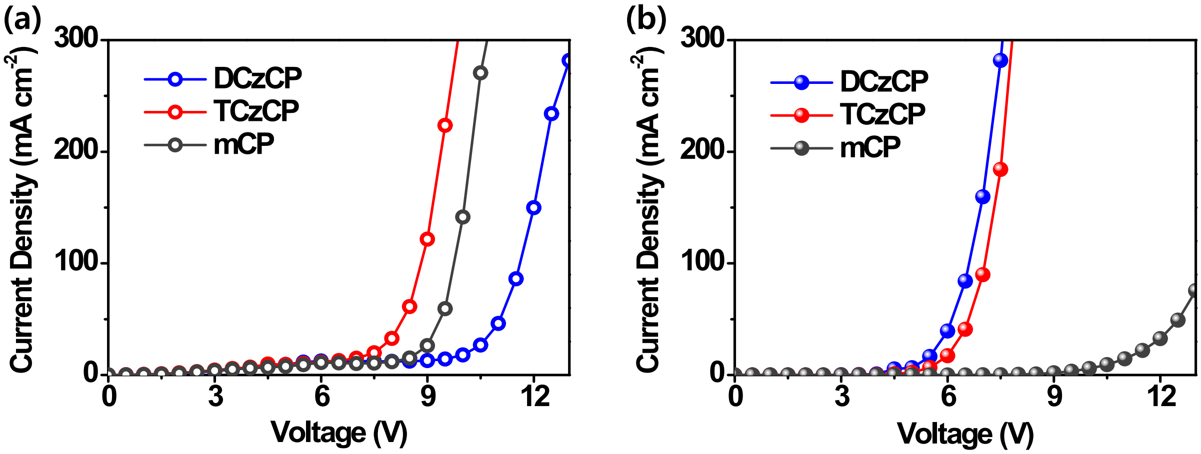

Fig. S8 (a) Hole only and (b) electron devices of **DCzCP**, **TCzCP**, and **mCP**.

8.0 Electroluminescence properties

In order to fabricate the solution-processable OLEDs, ITO (150-nm-thickness) coated glass substrates with a sheet resistance of 10 Ω cm^{-2} and an active pattern size of 2 × 2 mm^2 were utilized. A known green TADF emitter, 2,4,5,6-tetrakis(3,6-di-tert-butyl-9H-carbazol-9-yl)isophthalonitrile (t4CzIPN),[7] and the newly synthesized materials, **DCzCP** and **TCzCP**, as hosts were executed in the emissive layer. The device configuration was used as follows: ITO (150 nm)/PEDOT:PSS (40 nm)/PVK (10 nm)/Host (DCzCP or TCzCP or mCP):t4CzIPN (20 nm, 4–6 wt%)/TPBi (40 nm)/LiF (0.8 nm)/Al (100 nm), where PEDOT:PSS is the hole injection layer, PVK is the hole transport layer, TPBi is an electron transport layer,[8] and LiF and Al are the electron injection layer and cathode, respectively. The dopant concentration was varied between 4.0 to 6.0 wt% in order to identify optimal dopant levels for improved device performance. The PEDOT:PSS layer was directly spin-coated on an ITO plate and annealed at 155 °C for 15 min; PVK dissolved in chlorobenzene was spin-coated on the PEDOT:PSS layer and annealed at 130 °C for 20 min to remove the residual solvent before depositing the emissive layer by spin-coating from a toluene solution. All three steps were executed under ambient conditions before moving the substrates into a vacuum chamber. Subsequently, TPBi, LiF, and Al were deposited using the thermal evaporator. The current density-voltage-luminance (*J*-*V*-*L*) data were collected using a Keithley SMU 236 instrument and a SpectraScan PR-655 colorimeter. All the measurements were carried out in ambient conditions without any protective encapsulation of the devices.

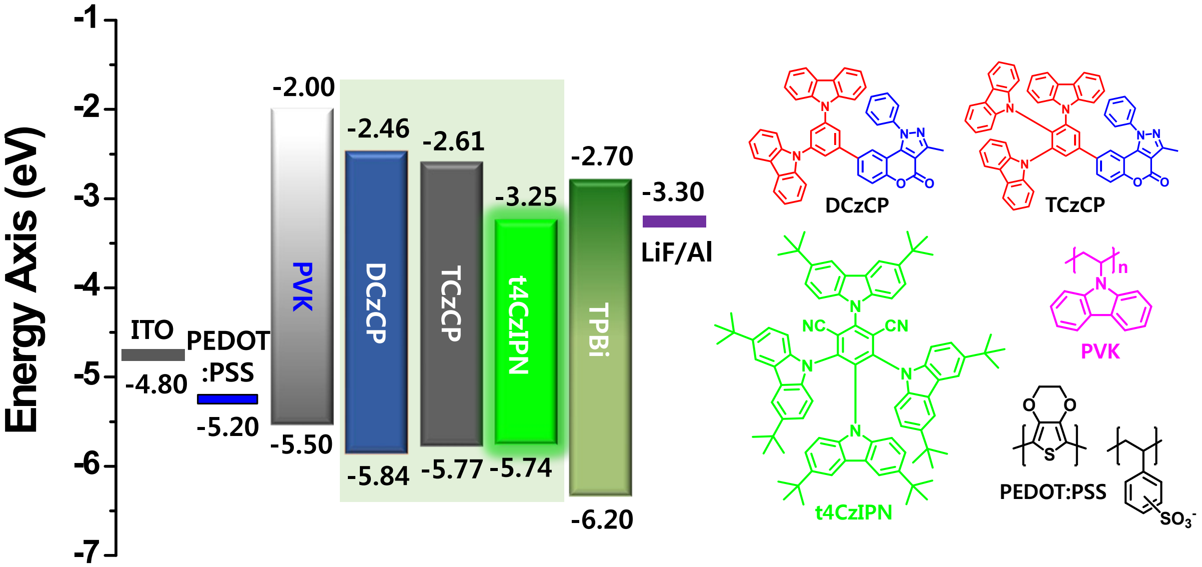

Fig. S9 Energy level diagram and the chemical structures of the materials used in this study.

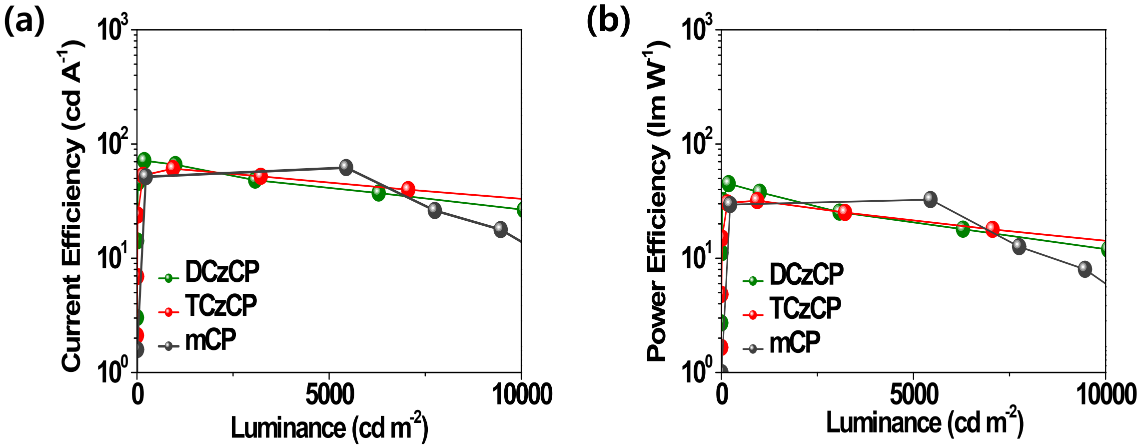

Fig. S10 Characteristics of green TADF-OLEDs for DCzCP:t4CzIPN, TCzCP:t4CzIPN and mCP:t4CzIPN: (a) current efficiency and (b) power efficiency versus luminance plots.

Table S3 Solution-processable green TADF-OLED performance data

Host	Dopant conc. (Wt%)	Quantum Efficiency (%)	Current Efficiency (cd/A)	Power Efficiency (lm/W)	CIE (x,y) [b]
		Max/500/1000 cd/m^2 [a]	Max/500/1000 cd/m^2 [a]	Max/500/1000 cd/m^2 [a]	
DCzCP	5.0	21.2/20.7/19.7	71.6/69.8/66.1	45.0/42.3/37.7	(0.31, 0.59)
TCzCP	5.0	18.4/17.0/18.3	61.0/56.7/60.6	31.9/31.1/31.8	(0.31, 0.58)
mCP	5.0	18.2/15.3/15.6	62.1/52.2/53.0	32.5/29.7/30.0	(0.32, 0.60)

[a] Maximum value, the value at 500 cd/m^2 and at 1000 cd/m^2 luminance. [b] CIE coordinates at a luminance of 1000 cd/m^2.

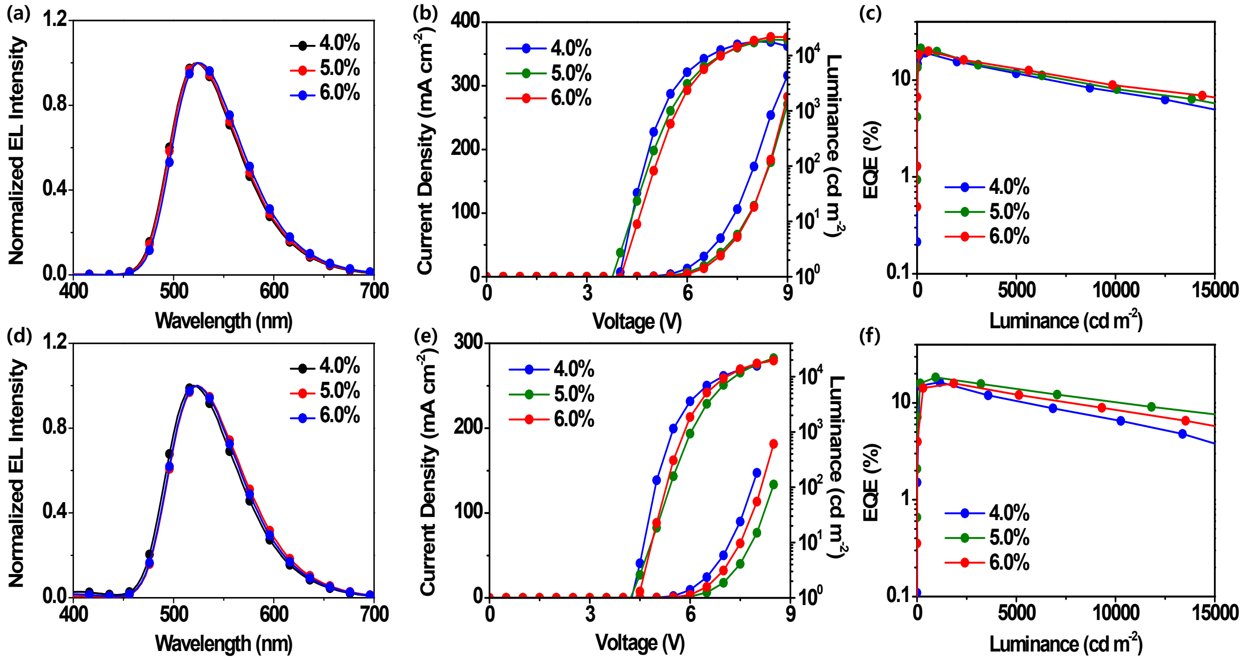

Fig. S11 Characteristics of TADF-OLED devices at various dopant concentrations for **DCzCP** (a, b, c) and **TCzCP** (d, e, f): (a and d) the normalized EL spectra (measured at 1000 cd m^{-2}), (b and e) *J–V–L characteristics*, and (c and f) EQE *versus* Luminance.

Table S4 Solution-processable green TADF-OLED performance data at various dopant concentrations

Host	Dopant conc. (Wt%)	EQE (%) [a]	CE (cd/A) [a]	PE (lm/W) [a]	CIE (x,y) [b]
DCzCP	4.0	19.1	64.5	40.5	(0.30, 0.59)
DCzCP	5.0	21.2	71.6	45.0	(0.31, 0.59)
DCzCP	6.0	19.9	67.7	39.5	(0.32, 0.59)
TCzCP	4.0	16.4	53.3	30.9	(0.30, 0.58)
TCzCP	5.0	18.4	61.0	31.9	(0.31, 0.58)
TCzCP	6.0	15.9	52.7	27.6	(0.31, 0.59)

[a] Maximum values. [b] At a luminance of 1000 cd/m^2.

Table S5 Comparison of the state-of-the-art performing solution-processed TADF OLEDs

S. No.	Host	Dopant	EQE_{max} (%)	EQE_{500} (%)	EQE_{1000} (%)	Roll-off (%)	Reference
1.	**DCzCP**	**t4CzIPN**	**21.2**	**20.7**	**19.7**	**7**	**Present work**
2.	CBP	TBP-DMA	22.1	--	20.3	8.0	9
3.	DCzPPy	DACT-II	30.8	29.0	27.0	12.0	10
4.	SiCz	t4CzIPN	18.3	~15.0	12.0	34	7
5.	mCPDPO	t4CzIPN	18.8	16.6	12.4	34	2
6.	mCP	4CzIPN	21.0	<16.0	<16.0	>24	11
7.	Cz-3CzCN	CzCzCN	23.8	~17.0	12.6	47	12
8.	Cz-3CzCN	Cz-4CzCN	23.5	~12.0	7.8	67	12
9.	mCP	COPO1	20.1	~10.0	~3.0	~85	13
10.	TPA-3/PO-T2T	9PhFDPhTz	24.0	15.5	10.1	58.0	14
11.	PVK:OXD-7	5	23.8	~18.0	16.5	31	15
12.	DPOBBPE	5CzCN	25.8	~19.0	~12.0	~53	16
13.	SiCz	4CzFCN	20.0	<1.0	--	--	17
14.	CzSi	MA-TA	22.1	--	--	--	18

Table S6 Comparison of the maximum performance and roll-off behavior at 1000 cd m^{-2} for t4CzIPN emitter fabricated through the solution as well as vacuum process

S. No.	Host	Dopant	Fabrication process	EQE$_{max}$ (%)	EQE$_{1000}$ (%)	Roll-off (%)	Reference
1.	**DCzCP**	**t4CzIPN**	**Solution**	**21.2**	**19.7**	**7.0**	**Present work**
2.	IAPC	t4CzIPN	Solution	19.2	17.5	9.0	19
3.	SiCT	t4CzIPN	Solution	19.2	12.4	36.0	20
4.	mCPDPO	t4CzIPN	Solution	18.8	12.4	34.0	2
5.	SiCz	t4CzIPN	Solution	18.3	12.0	34.0	7
6.	SiCz	t4CzIPN	Vacuum	17.1	13.5	21.0	7
7.	PE-PCzP	t4CzIPN	Solution	17.1	16.5	4.0	21

9.0 Device lifetime data

Besides high device efficiency, long operational lifetime is a crucial requirement for the practical application of OLEDs. The device lifetime predominantly depends on the stability of the chemical bonds (high bond dissociation energy), glass transition temperature (T_g), and electrochemical stability of the materials.

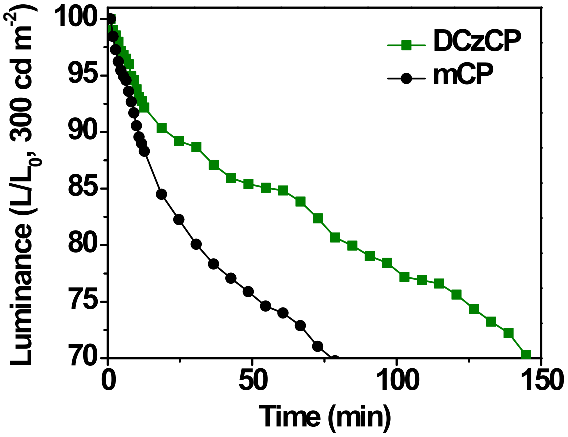

Fig. S12 Lifetime curves of OLEDs with DCzCP or mCP as a host at an initial luminance of 300 cd m^{-2}.

10. Notes and references

1. M. Godumala, S. Choi, S. Y. Park, M. J. Cho, H. J. Kim, D. H. Ahn, J. S. Moon, J. H. Kwon and D. H. Choi, *Chem. Mater.*, 2018, **30**, 5005-5012.
2. M. Godumala, S. Choi, S. K. Kim, S. W. Kim, J. H. Kwon, M. J. Cho and D. H. Choi, *J. Mater. Chem. C,* 2018, **6**, 10000-10019.
3. G. Xie, D. Chen, X. Li, X. Cai, Y. Li, D. Chen, K. Liu, Q. Zhang, Y. Cao and S.-J. Su, *ACS Appl. Mater. Interfaces,* 2016, **8**, 27920−27930.
4. S. Y. Lee, T. Yasuda, H. Komitama, J. Lee and C. Adachi, *Adv. Mater.*, 2016, **28**, 4019-4024.
5. J. S. Kang, T. R. Hong, H. J. Kim, Y. H. Son, R. Lampande, B. Y. Kang, C. Lee, J. K. Bin, B. S. Lee, J. H. Yang, J. W. Kim, S. Park, M. J. Cho and D. H. Choi, *J. Mater. Chem. C*, 2016, **4**, 4512-4520.
6. J. Pommerehne, H. Vestweber, W. Guss, R. F. Mahrt, H. Bassler, M. Porsch and J. Daub, *Adv. Mater.,* 1995, **7**, 551−554.
7. Y. J. Cho, K. S. Yook and J. Y. Lee, *Adv. Mater.*, 2014, **26**, 6642-6646.
8. G. Hughes and M. R. Bryce, *J. Mater. Chem.*, 2005, **15**, 94-107.
9. X. Cai, D. Chen, K. Gao, L. Gan, Q. Yin, Z. Qiao, Z. Chen, X. Jiang and S.-J. Su, *Adv. Funct. Mater.*, 2018, **28**, 1704927-1704935.
10. K.-W. Tsai, M.-K. Hung, Y.-H. Mao and S.-A. Chen, *Adv. Funct. Mater.*, 2019, **29**, 1901025.
11. T. Zhou, G. Xie, S. Gong, M. Huang, J. Luo and C. Yang, *ACS Appl. Mater. Interfaces*, 2017, **9**, 34139-34145.
12. X. Ban, A. Zhu, T. Zhang, Z. Tong, W. Jiang and Y. Sun, *Chem. Commun.*, 2017, **53**, 11834-11837.
13. Z. Ren, R. S. Nobuyasu, F. B. Dias, A. P. Monkman, S. Yan and M. R. Bryce, *Macromolecules*, 2016, **49**, 5452-5460.
14. J. Zhao, C. Zheng, Y. Zhou, C. Li, J. Ye, X. Du, W. Li, Z. He, M. Zhang, H. Lin, S. Tao and X. Zhang, *Mat. Horizons*, 2019, DOI: 10.1039/c9mh00373h.
15. W.-P. To, D. Zhou, G. S. M. Tong, G. Cheng, C. Yang and C.-M. Che, *Angew. Chem. Int. Ed*., 2017, **56**, 14036-14041.
16. S. K. Jeon, H.-J. Park and J. Y. Lee, *ACS Appl. Mater. Interfaces*, 2018, **10**, 5700-5705.
17. Y. J. Cho, B. D. Chin, S. K. Jeon and J. Y. Lee, *Adv. Funct. Mater.*, 2015, **25**, 6786-6792.
18. Y. Wada, S. Kubo and H. Kaji, *Adv. Mater.*, 2018, **30**, 1705641-1705648.
19. C. H. Jeong, M. Godumala, J. Yoon, S. Choi, Y. W. Kim, D. H. Choi, M. J. Cho and D. H. Choi, *ACS Appl. Mater. Interfaces,* 2019, **11**, 17602-17609.

20. S. Choi, J. Yoon, M. Godumala, H. J. Kim, S. H. Park, S. K. Kim, H. Lee, J. H. Kwon, M. J. Cho and D. H. Choi, *Dyes and Pigments,* 2019, **167** 120-126.
21. S. Shao, S. Wang, X. Xu, Y. Yang, J. Lv, J. Ding, L. Wang, X. Jing and F. Wang, *Macromolecules*, 2019, **52**, 3394-3403.